Since January 2020 Elsevier has created a COVID-19 resource centre with free information in English and Mandarin on the novel coronavirus COVID-19. The COVID-19 resource centre is hosted on Elsevier Connect, the company's public news and information website.

Biosensors and Bioelectronics 219 (2023) 114816

Contents lists available at ScienceDirect

Biosensors and Bioelectronics

journal homepage: www.elsevier.com/locate/bios

An ultrasensitive and rapid "sample-to-answer" microsystem for on-site monitoring of SARS-CoV-2 in aerosols using "*in situ*" tetra-primer recombinase polymerase amplification

Shanglin Li [a,1], Bao Li [a,1], Xinyue Li [b,1], Ce Liu [c,1], Xiao Qi [d], Yin Gu [e], Baobao Lin [a], Lingli Sun [d], Lan Chen [f,g], Bingqian Han [a], Jiazhen Guo [h], Yanyi Huang [i], Shuangsheng Wu [j], Lili Ren [f,g], Jianbin Wang [k], Jingwei Bai [c,****], Jianxin Ma [d,***], Maosheng Yao [b,**], Peng Liu [a,*]

[a] *Department of Biomedical Engineering, School of Medicine, Tsinghua University, Beijing, 100084, China*
[b] *State Key Joint Laboratory of Environmental Simulation and Pollution Control, College of Environmental Sciences and Engineering, Peking University, Beijing, 100871, China*
[c] *School of Pharmaceutical Sciences, Tsinghua University, Beijing, 100084, China*
[d] *Center for Disease Control and Prevention of Chaoyang District of Beijing, Beijing, 100021, China*
[e] *State Key Laboratory of Space Medicine Fundamentals and Application, China Astronaut Research and Training Center, Beijing, 100094, China*
[f] *NHC Key Laboratory of Systems Biology of Pathogens and Christophe Mérieux Laboratory, Institute of Pathogen Biology, Chinese Academy of Medical Sciences & Peking Union Medical College, Beijing, 100050, China*
[g] *Key Laboratory of Respiratory Disease Pathogenomics, Chinese Academy of Medical Sciences and Peking Union Medical College, Beijing, 100050, China*
[h] *Beijing Ditan Hospital, Capital Medical University, Beijing, 100015, China*
[i] *Biomedical Pioneering Innovation Center (BIOPIC), School of Life Sciences, Peking University, Beijing, 100871, China*
[j] *Institute for Infectious Disease and Endemic Disease Control, Beijing Center for Diseases Prevention and Control, Beijing, 100013, China*
[k] *School of Life Sciences, Tsinghua-Peking Center for Life Sciences, Tsinghua University, Beijing, 100084, China*

ARTICLE INFO

Keywords:
Aerosol
SARS-CoV-2
COVID-19
Filter paper
Recombinase polymerase amplification
Microfluidics

ABSTRACT

Airborne transmissibility of severe acute respiratory syndrome coronavirus 2 (SARS-CoV-2) has highlighted the urgent need for aerosol monitoring of SARS-CoV-2 to prevent sporadic outbreaks of COVID-19. The inadequate sensitivity of conventional methods and the lack of an on-site detection system limited the practical SARS-CoV-2 monitoring of aerosols in public spaces. We have developed a novel SARS-CoV-2-in-aerosol monitoring system (SIAMs) which consists of multiple portable cyclone samplers for collecting aerosols from several venues and a sensitive "sample-to-answer" microsystem employing an integrated cartridge for the analysis of SARS-CoV-2 in aerosols (iCASA) near the sampling site. By seamlessly combining viral RNA extraction based on a chitosan-modified quartz filter and "*in situ*" tetra-primer recombinase polymerase amplification (tpRPA) into an integrated microfluidic cartridge, iCASA can provide an ultra-high sensitivity of 20 copies/mL, which is nearly one order of magnitude greater than that of the commercial kit, and a short turnaround time of 25 min. By testing various clinical samples of nasopharyngeal swabs, saliva, and exhaled breath condensates obtained from 23 COVID-19 patients, we demonstrate that the positive rate of our system was 3.3 times higher than those of the conventional method. Combining with multiple portable cyclone samplers, we detected 52.2% (12/23) of the aerosol samples, six times higher than that of the commercial kit, collected from the isolation wards of COVID-19 patients, demonstrating the excellent performance of our system for SARS-CoV-2-in-aerosol monitoring. We envision the broad application of our microsystem in aerosol monitoring for fighting the COVID-19 pandemic.

* Corresponding author. Department of Biomedical Engineering, School of Medicine, Tsinghua University, Haidian District, Beijing, 100084, China.
** Corresponding author. College of Environmental Sciences and Engineering, Peking University, Haidian District, Beijing, 100871, China.
*** Corresponding author. Center for Disease Control and Prevention of Chaoyang District of Beijing, Chaoyang District, Beijing, 100021, China.
**** Corresponding author. School of Pharmaceutical Sciences, Tsinghua University, Haidian District, Beijing, 100084, China
E-mail addresses: jingwbai@mail.tsinghua.edu.cn (J. Bai), mice1125@163.com (J. Ma), yao@pku.edu.cn (M. Yao), pliu@tsinghua.edu.cn (P. Liu).
[1] Joint first authors with equal contributions.

https://doi.org/10.1016/j.bios.2022.114816
Received 15 June 2022; Received in revised form 22 September 2022; Accepted 12 October 2022
Available online 17 October 2022

1. Introduction

Transmission of severe acute respiratory syndrome coronavirus 2 (SARS-CoV-2) among people occurs mainly through exposure to respiratory fluids that contain infectious virus (Prather et al., 2020). People can release droplets and aerosols by coughing, sneezing, and some normal exhalation behaviors such as breathing, speaking, and singing (Alsved et al., 2020; Morawska and Milton, 2020; Stadnytskyi et al., 2020). After quickly evaporating into droplet nuclei, SARS-CoV-2 aerosols can float and be transported over long distances (Morawska et al., 2009), remain viable and infectious for several hours (van Doremalen et al., 2020), accumulate in enclosed spaces, and be inhaled deep into the lungs leading to more severe infection (Chu et al., 2020; Milton, 2020). The emergence of new SARS-CoV-2 variants, Delta (Planas et al., 2021) and Omicron (Karim and Karim, 2021), which have higher airborne transmissibility, have prompted the urgent need for monitoring of SARS-CoV-2 aerosols. Routinely monitoring SARS-CoV-2 aerosols at hotspot locations will contribute to the early warning capability of a COVID-19 outbreak, the effective restraint of the transmission chain, rapid work resumption, and the well-organized reopening of schools (Liu et al., 2020; van Doremalen et al., 2020).

Unfortunately, effective detection of SARS-CoV-2 in aerosols is not as easy as the routine analysis of human clinical samples. First, SARS-CoV-2 in aerosols is usually present at a low concentration ranging from 1 to 10 viruses/m^3 (Liu et al., 2020). Supposing a sampler with a flow rate of 100 L/min is used for aerosol collection, the final concentration of viruses in the solution is often less than 30 copies/mL after half an hour of sampling, which is far below the limit of detection (LOD) of commercially available kits (Pokhrel et al., 2020). Second, the analysis of aerosol samples should be carried out on-site with a short turnaround time. In this way, immediate actions, such as tracing close contacts and disinfecting contaminated space, can be conducted timely once SARS-CoV-2 is found in aerosols. However, current tests of SARS-CoV-2 heavily rely on centralized laboratories and specialized personnel for nucleic acid extraction and thermal cycling, which in turn slows down the assay and is not fit for on-site aerosol monitoring. There is an urgent need to develop a sensitive, rapid, and automatic molecular diagnosis platform that can be coupled to a highly efficient aerosol sampler to detect SARS-CoV-2 in aerosols.

Fully integrated instruments such as GeneXpert® (Cepheid), FilmArray® (BioFire®), and cobas® (Roche) have been developed and commercialized for the automated diagnosis of infectious diseases before the COVID-19 pandemic (Li, Z. et al., 2021). However, the sensitivities of these systems, which are either inferior to or close to that of commercial kits based on RT-qPCR, are insufficient for viral aerosol analysis. To simplify the structure of the instrument and shorten the testing time, isothermal amplification technologies such as recombinase polymerase amplification (RPA) (Cherkaoui et al., 2021), loop-mediated isothermal amplification (LAMP) (He et al., 2021), and rolling circle amplification (RCA) (Chaibun et al., 2021) have been invented and employed for SARS-CoV-2 detection (Esbin et al., 2020). However, the limits of detection (LOD) of these isothermal amplification systems are insufficient for viral aerosol analysis. Improving the LOD of these isothermal amplification technologies will aid in addressing the challenges faced by the on-site detection of infectious viruses in aerosols.

In the current study, we present the development of a novel SARS-CoV-2-in-aerosol monitoring system (SIAMs) which consists of portable cyclone samplers for collecting and concentrating aerosols from venues and an ultrasensitive "sample-to-answer" microsystem that can be deployed nearby for analyzing collected aerosol samples. Besides the highly efficient collection of aerosols from an enclosed space by the aerosol sampler, the newly developed "sample-to-answer" microsystem employing an integrated microfluidic cartridge for analysis of SARS-CoV-2 in aerosols (iCASA) can provide ultra-high sensitivity of 20 copies of viruses per mL, which is nearly one order of magnitude better than conventional RT-qPCR, and a rapid turnaround time of 25 min. The excellent performance of the SIAMs was demonstrated through analysis using mock samples and clinical samples. We envision that SIAMs will play a critical role in the detection and early warning of a COVID-19 epidemic, breaking the transmission chain, and the resumption of work and schools.

2. Methods and materials

2.1. Chemicals and reagents

Chitosan (medium molecular weight), lithium acetate (LiAc), urea, magnesium acetate ($MgAc_2$), and glycidoxypropyltrimethylsilane (GPTMS) were all purchased from Sigma-Aldrich. 2-(N-morpholino)-ethanesulfonic acid (MES), EDTA standard solution, yeast tRNA, and dithiothreitol (DTT) were purchased from Shanghai Macklin Biochemical, China. Diethylpyrocarbonate-treated water (DEPC water) and TE buffer (Tris-EDTA, pH 9.0) were obtained from Beyotime Biotechnology (Shanghai, China). The quartz filter paper was obtained from Whatman (Ø 47 mm, QMA). All solutions were prepared in water purified to 18.2 MΩ cm by Milli-Q Advantage A10.

2.2. Fabrication of iCASA

Both the 3D block and the planar chip were made of poly methyl methacrylate (PMMA) and fabricated using a CNC milling machine. The air sac of the iCASA was formed by sealing the niche on one side of the block with a piece of the rubber film. The fabrication process of the non-adhesive patterns and punched holes on the double-sided adhesive tape (DS tape) with an acrylic foam base (4910 VHB, 3M) is shown in Fig. S4. The assembled iCASA should be kept at room temperature for at least 24 h before use to achieve maximum adhesive strength of the tape.

2.3. Tetra-primer recombinase polymerase amplification (tpRPA) for detecting SARS-CoV-2 RNA

The sequences of the SARS-CoV-2 were obtained from the National Center for Biotechnology Information database (NCBI Reference Sequence: NC_045512.2). The primers and the probes in the tpRPA were designed using the online Primer-BLAST program (https://www.ncbi.nlm.nih.gov/tools/primer-blast). All the primers and the probes were synthesized and purified using HPLC by Shanghai Sangon Biotech, China. The tpRPA was performed using the Rapid Isothermal Amplification kit (Amplification Future Biotech., Yantai, China) with the primer listed in Supplementary Table 1 targeting the open reading frame 1a and 1b (ORF1ab) of SARS-CoV-2. The RPA reaction in PCR tubes was carried out at 42 °C for 30 min on the iCASA system and a Bio-rad CFX96 Touch™ Real-Time PCR Detection System.

2.4. Preparation of chitosan-modified filter paper

In the process of chitosan modification, a 10 × 2 cm^2 large piece of quartz filter paper (Ø 47 mm, QMA, Whatman, GE Healthcare, Pittsburgh, PA) was first activated with a piraña solution (H_2SO_4:H_2O_2, 7:3, v/v) for 30 min. After washing with deionized water (DI water) three times, the treated filter paper was submersed into a chitosan solution (0.05% (w/v) in 0.1% acetic acid, pH 6.0). After a 5-min incubation, 1.67% (v/v) GPTMS was added to the solution and reacted at room temperature overnight on a tube roller. The filter paper was then washed three times with DI water and dried completely at 50 °C in a vacuum drying oven. The chitosan-modified filter paper was sealed in a plastic bag and stored in a dryer until use. When needed, 3.5-mm-diameter discs of chitosan-modified filter paper were punched off using a manual puncher and then assembled into the iCASA at room temperature.

2.5. Optimization of lysis buffer for RNA extraction

Standard RNA templates containing the N gene of SARS-CoV-2 were prepared for optimizing and measuring the isolation efficiency of chitosan-modified filter paper for viral RNA extraction using a probe-based RT-qPCR assay based on the N2 target of the CDC assay (Holshue et al., 2020). RT-qPCR was performed using One Step PrimeScript™ III RT-qPCR Mix (TAKARA) with the following primers: the forward primer 5′-TTA CAA ACA TTG GCC GCA AA-3′ and the reverse primer 5′-GCG CGA CAT TCC GAA GAA-3′. The RT-qPCR assay was run using a TaqMan™ probe with the following sequence: 5′-FAM-ACA ATT TGC CCC CAG CGC TTC AG-BHQ1-3′. All the PCR assays were carried out on the Bio-rad CFX96 System with an RT step of 52 °C for 5 min followed by 45 cycles with a denaturing step of 95 °C for 5 s and an annealing and elongation step of 60 °C for 30 s. We evaluated the performance of the chitosan-modified filter paper combined with the tetra-primer RPA for the detection of viral RNA using 2019-nCoV RNA reference material (National Institute of Metrology, China).

2.6. Preparation and operation of iCASA

Before the analysis of samples, 30 μL of RPA reagents were loaded into the reagent reservoir using a 100-μL microsyringe and 1.5 μL of magnesium acetate ($MgAc_2$) solution was pre-dried in the Mg^{2+} reservoir at 50 °C. Before sample loading, 0.5 mL of 2X lysis buffer containing 2 μg/mL of yeast tRNA was loaded into the sample reservoir. Then, 0.5 mL of these samples were directly pipetted into the sample reservoir, where the samples were mixed with the lysis buffer. For aerosol samples, the collected samples were directly transferred into the sample reservoir. After loading reagents and samples, the chip was sealed with rubber plugs and placed in the cartridge tray of the instrument. The remainder of the analytical processes was performed automatically without any manual operations.

2.7. System characterization using quality control reference materials

The LOD of iCASA was determined using the commercially available SARS-CoV-2 pseudoviral RNA weak positive quality control reference material (National Institute of Metrology, China) containing the complete N gene, the complete E gene, and a segment of ORF1ab gene. For highly sensitive detection of SARS-CoV-2, the sensitivity was evaluated using 1 mL of 1x lysis buffer with 1 μg/mL of yeast tRNA containing 1,000, 200, 100, 50, and 20 copies of SARS-CoV-2 pseudoviral RNA. After preparing the sample solution, the mixture was loaded into the iCASA and analyzed automatically. The reaction time of tetra-primer RNA was 20 min.

2.8. Analysis of nasopharyngeal swabs, saliva, exhaled breath condensates, air outlet swabs, and aerosol samples

To evaluate the performance of our system, a total of 23 nasopharyngeal swab samples, 18 saliva samples, 20 exhaled aerosols and droplets (EBC) samples, 21 surface swab samples of air outlets, and 23 aerosol samples were collected at Beijing Ditan Hospital, Capital Medical University by the colleagues from the Center for Disease Control and Prevention of Chaoyang District of Beijing with informed consents from patients. Samples of exhaled breath condensate were collected from COVID-19 patients using a BioScreen II device (Beijing BioCTech, Beijing, China) for 5 min. Aerosols were collected from isolation wards using a portable cyclone sampler for 30 min. The surface swab samples of air outlets were collected by swirling the cotton swabs wetted with viral transport media (VTM) for 3 cycles on the surfaces of the air outlets in the isolation wards. Then, the swabs were transferred into VTM for storage. Before the on-chip analysis, all samples were incubated at 56 °C for 30 min to inactivate viruses. A volume of 500 μL of the nasopharyngeal swab, saliva, surface swab, and EBC samples, and 1 mL of aerosol samples were loaded into the iCASA and the viral RNA of SARS-CoV-2 was tested automatically in the "sample-to-answer" microsystem. To compare with traditional testing based on RT-PCR, we extracted RNA from 200 μL of each sample and tested these samples a commercial detection kit (Jiangsu Bioperfectus Technologies, Nanjing, China) with primers and probes targeting the *ORF1ab* and *N* genes of SARS-CoV-2.

3. Results and discussion

3.1. Collection of bioaerosols using high-flow portable cyclone samplers

The SIAMs consists of portable cyclone samplers for collecting aerosols into a collection tube with 2 mL of lysis buffer and a sensitive "sample-to-answer" microsystem with eight throughputs for detecting highly diluted viruses collected in the lysis buffer. Multiple aerosol samplers can be simultaneously deployed in several small rooms or several spots in a large public indoor space to collect aerosols. After unloading the collection tube, the tube can directly screwed onto a disposable cartridge, which can then put into the analyzer deployed nearby for the on-site and automated nucleic acid analysis. This sample loading process minimizes potential risks of infection and makes the process easy to operate without pipetting (Fig. 1A).

The airborne particle collection was conducted using a portable cyclone sampler described previously (Li, X. et al., 2021). While air swirls within the cyclone pipe, the particles hit the pipe wall due to the centrifugal force induced by the swirling motion and fall to the collection tube (Fig. S1A). By collecting the polystyrene latex (PSL) microspheres that were aerosolized using a BGI Collison Nebulizer (Mesa Labs) (Fig. S1B), the cutoff size (d_{50}) of the sampler was determined to be 0.806 μm, at which the collection efficiency was 50% (Fig. 1C and Table S1), and the collection efficiency reached nearly 100% when the size increased 2.371 μm. To ensure the safety of the sampling staff during the aerosol collection, we directly used the lysis buffer for collecting aerosols and measured the viral activation of the lysis buffer. Compared with the control, the N gene concentration of SARS-CoV-2 D614G in P1 Vero cells decreased significantly after incubation with SARS-CoV-2 D614G of different dilutions (1:100, 1:500 first treated with 1X lysis buffer), and almost no viral RNA was detected in P2 or P3 Vero cells, illustrating that this collection solution sufficiently inactivated viruses (Fig. S2).

3.2. "Sample-to-answer" cartridge following "3D extensible" design paradigm

For monitoring the SARS-CoV-2 aerosols at congregate settings, we developed the ultrasensitive "sample-to-answer" microsystem based on an integrated cartridge. By following a "3D extensible" microfluidic design paradigm presented previously by our group (Geng et al., 2019, 2020), we developed the slim, cassette-like iCASA with dimensions of 87 × 15 × 50 mm, which consisted of a three-dimensional block, a piece of double-sided adhesive tape, and a planar chip ((Fig. 1B and S3)). The block with milliliter-scale drilled reservoirs representing the macroscale section of the cassette was employed for storing reagents and collecting waste. The planar chip with microliter-scale channels and chambers representing the microscale portion was used for precise liquid transportation, nucleic acid extraction, and amplification reaction. The block and the chip were permanently bonded together using a piece of adhesive tape (DS tape, 4910 VHB, 3M) with pre-defined non-adhesive patterns and punched holes for valve structures. The design provides the microfluidic cartridge with the capability of processing both microliter- and nanoliter-scale solutions simultaneously, which is critical for analyzing large-volume samples. To fully enclose the entire cartridge, an air sac was designed on the side of the block. With a small vent groove on the sidewall of the waste reservoir to the air sac, the air was expelled from the cartridge into the sac during the plunger driving process. In addition, the sample reservoir was also used as a collection tube in the

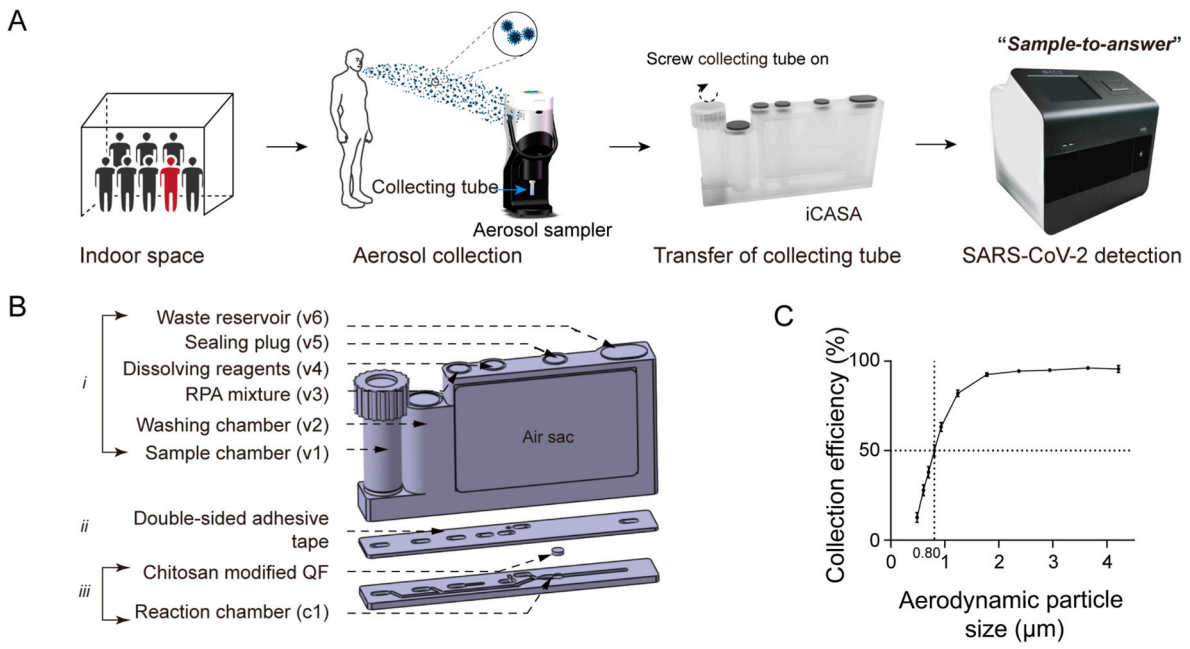

Fig. 1. Schematic illustration of the SIAMs. (A) The workflow of the SIAMs includes the sample collection with a portable cyclone sampler followed by detection on an ultrasensitive "sample-to-answer" microsystem. (B) The structure of the disposable iCASA consists of a three-dimensional block (*i*), a piece of double-sided adhesive tape (*ii*), and a planar chip (*iii*). (C) Physical collection efficiency curves of the aerosol sampler when collecting polystyrene latex microspheres with different sizes ranging from 0.487, 0.604, 0.698, 0.806, to 4.217 μm.

aerosol sampler and a detachable tube was used to transfer samples from the sampler to the cartridge (Fig. S3C).

The structure and the operation of the iCASA is shown in Fig. 1A and S6. Firstly, 1 mL of the viral lysis buffer containing the collected aerosols was injected from the sample reservoir through a check valve (in) into the reaction chamber (c1) by the plunger. At this step, the viral RNA was captured by a piece of filter paper embedded in the reaction chamber. After washing the filter paper with diethylpyrocarbonate (DEPC) water from the washing reservoir, RPA reagents stored in the reagent reservoir were injected into the Mg^{2+} reservoir to dissolve the pre-dried $MgAc_2$ and initiate the RPA reaction. The initiated RPA reaction reagents were then further driven into the reaction chamber, where the targeted viral RNA captured by the filter paper was amplified *in situ,* and the fluorescence signal was detected by the instrument. During the entire operation, all the waste was collected in the waste reservoir and the air pressure change was balanced by the air sac on the side of the chip. Up to eight chips could be loaded side by side into control and detection instrument. The detailed 3D structure of the instrument shown in Fig. 4A and S5 contains a CNC (computer numerical control) plunger array for fluid actuation, electronics for temperature control, and optics for fluorescence detection.

3.3. Chitosan-modified filter paper for highly efficient extraction and enrichment of viral RNA

Degradation of the viral RNA during the sample pretreatment and hyperthermia inactivation, inadequate elution of the captured RNA, and confined sample volume of the amplification reaction system led to deficiencies of viral RNA during the processes of viral-RNA extraction and amplification, which seriously decreased the total sensitivity of nucleic acid amplification tests (NAATs) based on RT-PCR. Our group previously demonstrated high efficient DNA extraction using a piece of chitosan-modified filter paper (Gan et al., 2017; Gu et al., 2019). Here, we utilized chitosan-modified filter paper which function as a solid-phase media to efficiently extract viral RNA. Since no elution step was performed, all the captured RNA on the filter was used for the amplification, leading to a significant improvement in the sensitivity. Unlike the conventional silica-based extraction methods employing a bind-wash-elute step (Höss and Pääbo, 1993), the chitosan-modified filter paper only used the capture and wash steps. The amplification reagents can be directly loaded and mixed with the filter paper for "*in situ*" amplification (Fig. 2A). At the capture step, negative-charged nucleic acids will be efficiently bound by the positive-charged fibers via electrostatic adsorption and the physical trapping effect. Interestingly, the chitosan-modified filter paper will firmly capture the nucleic acid under physical trapping and prevent the elution of captured DNA by the wash buffer and the loading reagents (Fig. 2A). By utilizing these characteristics of the chitosan-modified filter paper, we effectively simplified the structure of the iCASA and dramatically improved the sensitivity of testing.

To optimize and evaluate the RNA extraction of the chitosan-modified filter paper, we designed a simplified microdevice with a single chamber containing the embedded filter paper. The device was reversibly sealed with a piece of tape (4905 VHB, 3M), so that the filter can be taken out from the chamber for the in-tube RT-qPCR after the RNA capture in the device (Fig. 2B). First, we optimized the pH value in the lysis buffer and found the Ct value reached the lowest of 31.7 when the pH of the buffer was 5.0 (Fig. 2C). Next, the use of carrier RNA is a common strategy to improve RNA extraction efficiency (Shaw et al., 2009). Here, we chose yeast tRNA as carrier RNA and optimized its input amount in the lysis buffer. With the increase of yeast tRNA from 0.4 to 2.0 μg/mL, the Ct values decreased from 36.5 to 35.0 (Fig. 2D). Considering too much carrier RNA could decrease the specificity of RPA, we chose 2.0 μg/mL of yeast tRNA in the lysis buffer for the following experiments. We next measured the enrichment ratio of chitosan-modified QF on the simplified device using 2000 copies of standard RNA templates in different volumes of the lysis buffer. The capture efficiencies of chitosan-modified fibers were reduced from 68.9%, 66.2%, and 44.8%, to 19.7% when the sample volume was increased from 0.2, 0.5, and 1.0, to 2.0 mL, respectively. Correspondingly, the enrichment ratio was 138, 331, 448, and 394 (Fig. 2E). Therefore, we chose 1.0 mL as the optimal sample volume since the enrichment ratio was the highest while the capture efficiency remained near 50%.

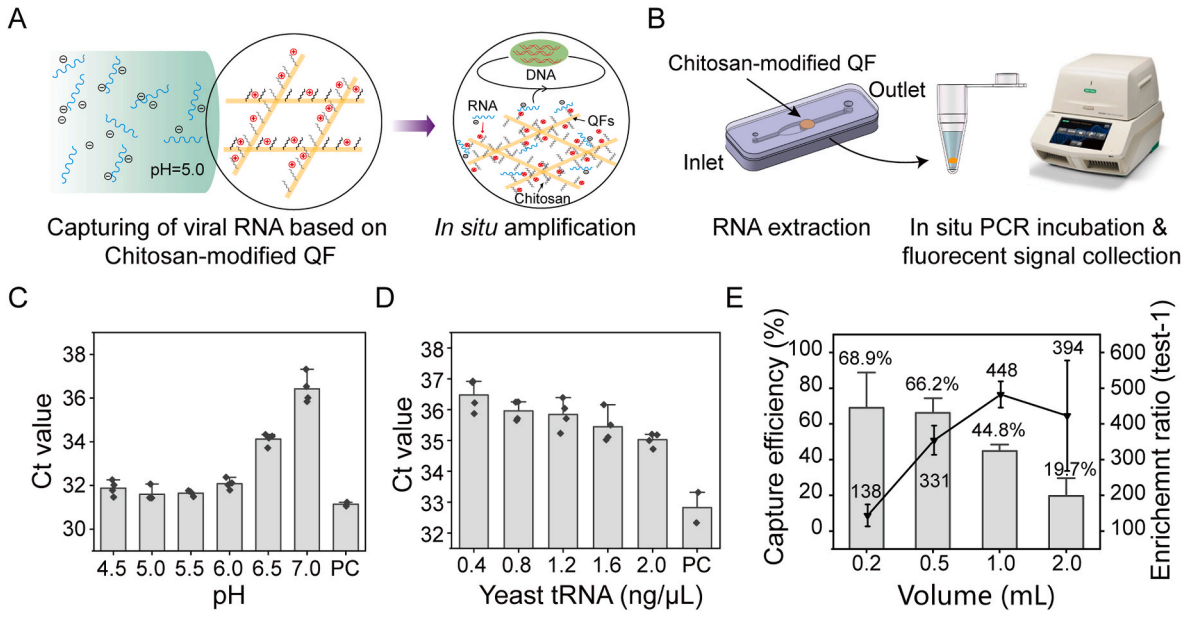

Fig. 2. Highly efficient extraction and enrichment of viral RNA by chitosan-modified filter paper. (A) Schematic of viral RNA extraction by chitosan-modified filter paper. (B) Experimental setup for the validation of RNA extraction efficiency. RNA extraction is performed on a simplified microdevice with a single chamber containing an embedded piece of filter paper. (C) Optimization of pH values of the lysis buffer ($n = 3$ independent repeats). (D) Optimization of yeast tRNA input in the lysis buffer ($n = 3$ independent repeats). (E) Capture efficiency and enrichment ratio of chitosan-modified filter paper for the extraction of viral RNA from different sample volumes ($n = 3$ independent repeats).

3.4. The tpRPA for ultrasensitive detection of SARS-CoV-2 RNA

Another restricting factor for ultrasensitive detection of viral RNA is the specificity and sensitivity of amplification. To increase the sensitivity and shorten the assay time, we developed a tpRPA system with four primers, an outside and an inside primer pair, that worked synchronously to amplify the target sequences efficiently instead of two primers in the conventional double-primer RPA (dpRPA) (Fig. 3A). In the tpRPA system, the sequences of the primers (Table S2) were carefully optimized to avoid primer dimers and the concentrations of the primers and probe were also optimized to achieve ultrasensitive detection (Fig. S7 and Fig. S8). We compared the tpRPA and the dpRPA in tubes using 20 copies of the standard reference materials of SARS-CoV-2 RNA in each 20-μL reaction system. Contrary to the barely distinguishable amplification curves of the positive and the negative tests in the dpRPA, the distinction between the positive and the negative tests of the tpRPA was much more remarkable (Fig. 3B). We then measured the LOD of the tpRPA in the tubes and found that even 5 copies of RNA could be distinguished (Fig. 3C and S9).

Next, when RNA extraction based on the chitosan-modified filter

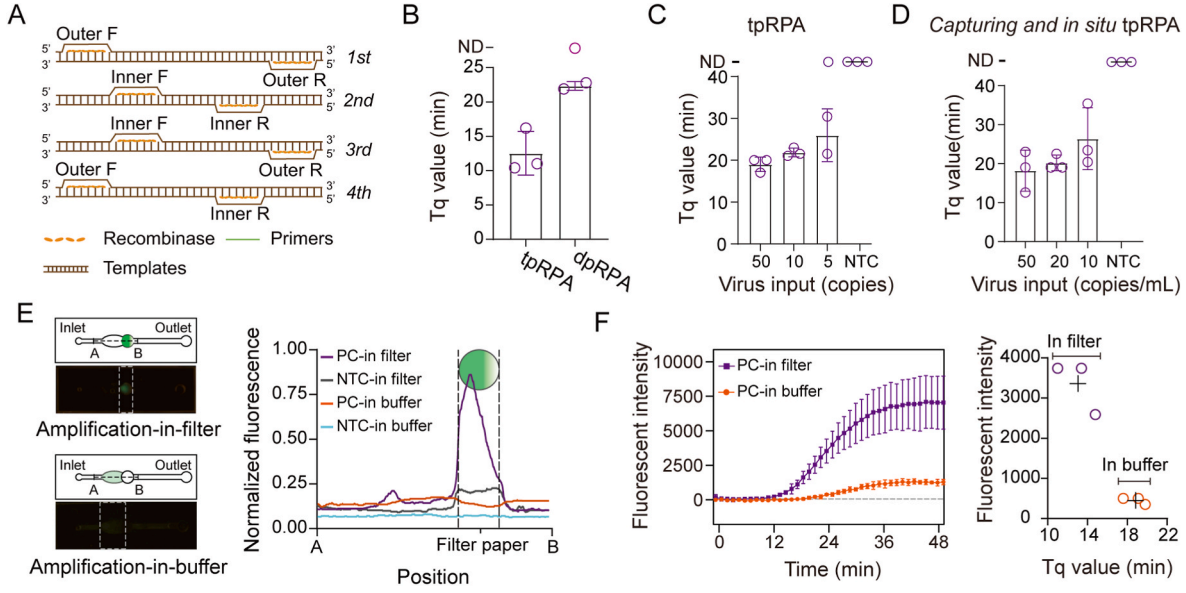

Fig. 3. The tpRPA for the ultrasensitive detection of SARS-CoV-2. (A) Schematic of tpRPA. Compared with the conventional dpRPA, the outside and the inside primer pairs amplify the template synchronously. (B) Comparison of tpRPA with dpRPA for detecting 20 copies of template. (C) The determination of the LOD of the tpRPA for detecting viral RNA. (D) The determination of the LOD of the viral RNA extraction based on the chitosan-modified glass filter coupled with *in situ* tpRPA for SARS-CoV-2 detection. (E) Distribution of fluorescent intensities along the dotted line AB in the fluorescent images. (F) Amplification curves and Tp values of amplification-in-filter and the amplification-in-buffer. ND: Not detectable.

paper was coupled with *in situ* tpRPA, we achieved the detection of 10-copies/mL viral RNA (Fig. 3D and S9). To better understand the "*in situ*" tpRPA, we compared the distributions of the amplicons in the reaction chambers between the amplification-in-filter ("*in situ*" RPA) and the amplification-in-buffer (conventional RPA), in which 200 copies of RNA template were either captured in the filter before the RPA reagent loading or filled into the reactor with the RPA reagents. As shown in Fig. 3E, the amplicons were highly concentrated within the filter, and the fluorescent signal was about 6 times higher than that in the chamber. By contrast, the amplification-in-buffer demonstrated a much more uniform distribution of the amplicons across the entire reactor (Fig. 3E and S10). This difference illustrates that the amplification mainly occurred within the filter where the template was captured, and the amplicons did not diffuse out freely. From the fluorescent amplification curves, we found the highly concentrated amplicons in the amplification-in-filter resulted in a shorter quantification time (Tq) (6 min) and a higher final fluorescent intensity (8-fold) than those in the amplification-in-buffer, illustrating significant advantages of the on-chip analysis (Fig. 3E and F).

In order to further evaluate the sensitivity of the iCASA, we loaded 1 mL of the viral lysis buffer containing different amounts of pseudoviruses from 1000 copies down to zero into the cartridges and evaluated the LOD of the iCASA system. As shown in Fig. 4C, compared with the unchanged fluorescence of the group of zero-copies pseudoviruses, the fluorescence signal of all three parallel groups of 20 copies/mL was significantly increased after 20 min of amplification, demonstrating the LOD of the iCASA system reached 20 copies/mL. In addition, the quantification time was also linearly correlated with the logarithm of viral concentration (R^2 is 0.997), illustrating the quantitative performance of our system.

3.5. Ultrafast and ultrasensitive detection of SARS-CoV-2 clinical samples using the iCASA

To validate the capability of our system for analyzing clinical samples, we obtained nasopharyngeal swab samples from 23 COVID-19 patients and analyzed these samples using the iCASA system together with the commercial kit based on RT-qPCR (Fig. S11). The total analytical time of our system including sample loading, extraction, and tpRPA was only 25 min (Fig. 4B). About 0.5 mL of each sample was first mixed with 0.5 mL of the viral lysis buffer and then loaded into the cartridge. In parallel, 0.5 mL of the sample was analyzed using the commercial kit based on magnetic bead-based RNA extraction and RT-PCR, which took about 2–3 h. The results demonstrated that the positive detection rate of our platform was 82.6% (19/23), which was significantly high than the 39.1% (9/23) of the commercial kit (Fig. 5 and S12). More importantly, all the samples that were found to be positive by the commercial kit were equally detected by our system, illustrating the excellent performance of our system.

Some studies have found that the analysis of saliva specimens can provide a similar sensitivity compared with nasopharyngeal swabs for COVID-19 diagnosis (Bastos et al., 2021). Here, we evaluated the performance of our platform for the SARS-CoV-2 detection in 18 saliva samples obtained from the same group of 23 patients. We achieved a 61.1% (11/18) positive detection rate using our system, while there was only one positive result using the commercial kit based on RT-qPCR (Fig. 5).

Since the transmission of SARS-CoV-2 is mainly through exhaled aerosols and droplets, the sampling of exhaled aerosols and droplets (EBC) is regarded as a promising noninvasive approach for the diagnosis of COVID-19 (Sawano et al., 2021). A BioScreen II device (Beijing Bio-CTech, Beijing, China) was employed to collect 20 EBC specimens from the same group of 23 patients following the protocols provided by the manufacturer. During the sampling process, a patient breathed normally through a disposable straw into an electrically cooled tube, in which air condenses to liquid. After gathering for 5 min, about 2 mL of EBC was collected (Fig. 5 and S12), and 0.5 mL of EBC samples were mixed with 0.5 mL of the lysis buffer and loaded into the iCASA for analysis. As a comparison, 0.2 mL of EBC samples were analyzed using the commercial kit independently. We achieved a 30% (6/20) positive detection rate for

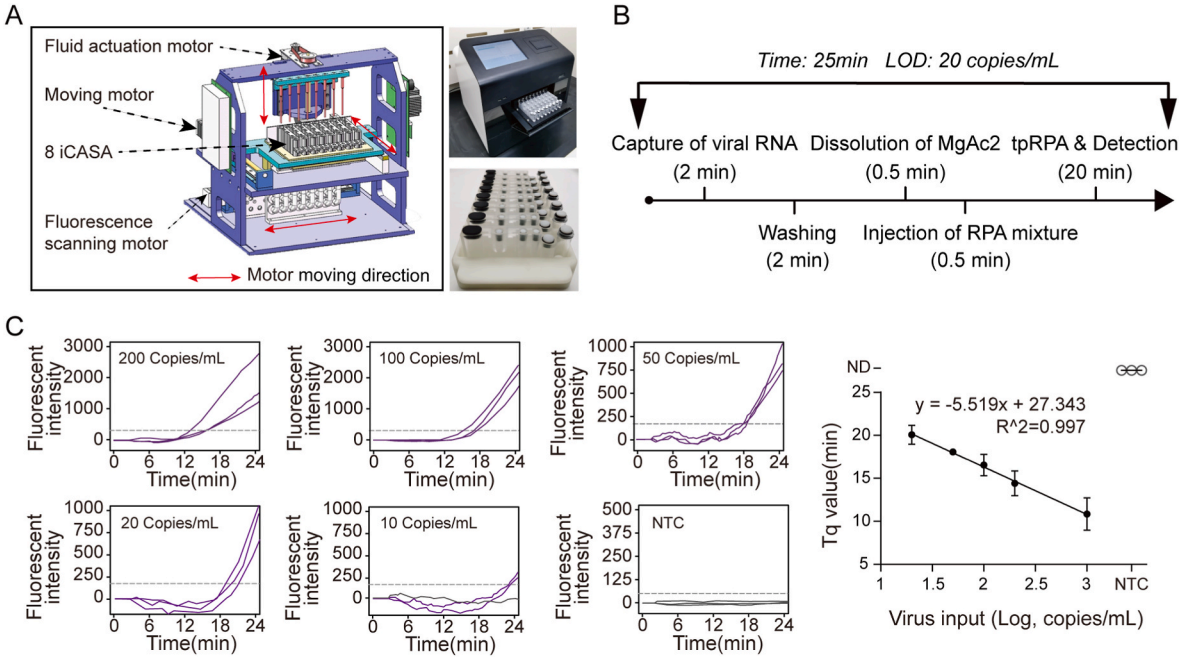

Fig. 4. Performance evaluation of the iCASA for the ultrasensitive detection of SARS-CoV-2 RNA. (A) The 3D structure of the integrated microsystem, including a moving motor, a fluid actuation motor, and a fluorescence scanning motor. Photos of the microsystem and eight iCASA mounted in the cartridge tray of the microsystem. (B) Timeline of the analytical procedure, including viral RNA capture, washing, dissolution of Mg^{2+} ions, injection of the RPA mixture, and tetra-primer RPA amplification. (C) The LOD of the iCASA for ultrasensitive detection of SARS-CoV-2 RNA. The LOD was measured using the quality control reference materials of SARS-CoV-2 diluted in the 1-mL buffer. NTC, Negative-template control. (n = 3, mean ± SD).

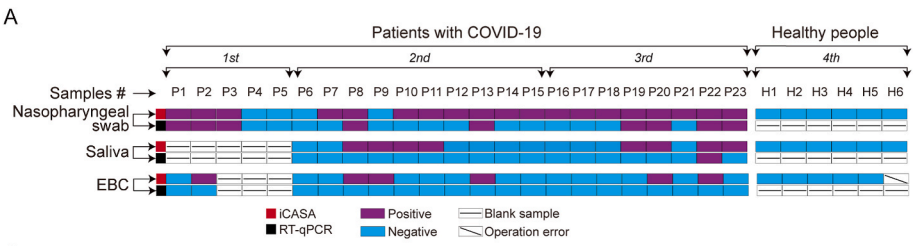

B

COVID-19 patients

	Positive	Negative	Error	Positive detection rate
iCASA	33/61	28/61	0/61	54.10%
RT-qPCR	10/61	51/61	0/61	16.39%

Negative samples

Positive	Negative	Error	False positive rate
0/18	17/18	1/18	0%

Fig. 5. Ultrasensitive detection of clinical samples using the iCASA. (A) Heatmap result of clinical SARS-CoV-2 samples analyzed using the iCASA, including 23 nasopharyngeal swab samples, 18 saliva samples, and 20 EBC samples collected from COVID-19 patients, as well as 17 negative samples collected from healthy volunteers. (B) Statistical results of clinical samples shows that the positive detection rate of the iCASA was more than three times that of the commercial kit based on RT-PCR.

the analysis of the EBC specimens in contrast to the all-negative results provided by the commercial kit, illustrating the better performance of our platform for the noninvasive diagnosis of COVID-19.

Our system is capable of detecting low levels of SARS-CoV-2 rapidly due to the following improvements: (i) The chitosan-modified filter paper was used for viral RNA extraction for up to 1 mL of samples and "*in situ*" amplification without elution; (ii) The tpRPA was developed to replace the conventional two-primer system so that both the sensitivity and the reaction speed were improved; (iii) The enrichment of amplicons and primers by chitosan modified filter paper increased the RPA reaction rate and reduced the detection time; (iv) The automated microsystem employed an integrated cartridge, in which the filter-based RNA extraction and the "*in situ*" tpRPA were seamlessly integrated, increasing the sensitivity by effectively using the initial reaction stage of tpRPA with the highest reaction efficiency.

3.6. *On-site monitoring of SARS-CoV-2 RNA in aerosols using the SIAMs*

Aerosol monitoring in hotspot sites, such as hospitals, airports, and conference centers is essential for severing transmission chains of COVID-19. However, it is still a big challenge because of the insensitive detection and the tedious analysis of SARS-CoV-2 aerosols. To evaluate the performance of SIAMs for the sensitive detection of viral aerosols, we simulated the bioaerosol generation, collection, and detection in a Class II A2 biosafety cabinet (Fig. 6A). Aerosols were generated using a medical compressed atomizer (DE-WY400; Shenzhen dedakj-health, Shenzhen, China) and collected using a portable cyclone sampler. We successfully detected viral RNA when the concentrations of the pseudovirus of SARS-CoV-2 were 10^4, 10^3, and 10^2 copies/mL, and the Tq values of these groups also had an approximately linear relationship (Fig. 6B and C), verifying the effectiveness of SIAMs for aerosol monitoring.

To further validate the feasibility of aerosol SARS-CoV-2 detection in

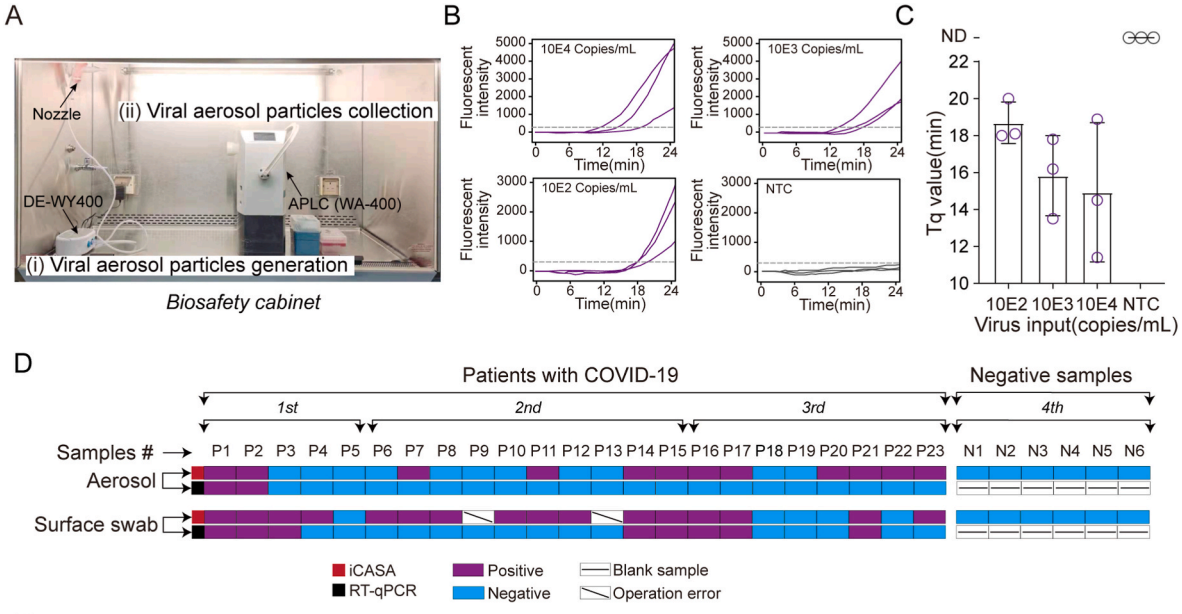

E

COVID-19 patients

	Positive	Negative	Error	Positive detection rate
iCASA	28/46	16/46	2/46	60.87%
RT-qPCR	10/46	36/46	0/46	21.74%

Negative samples

Positive	Negative	Error	False positive rate
0/12	12/12	0/12	0%

Fig. 6. Ultrasensitive detection of SARS-CoV-2 in aerosols using the SIAMs. (A) Photograph of the experimental setup of the generation and collection of SARS-CoV-2 aerosols in a class II A2 biosafety cabinet. (B) Amplification curves of mock aerosol samples generated from different viral concentrations of 10^4, 10^3, and 10^2 copies/mL. The experiments are repeated three times. (C) Tq values of mock aerosol samples at different viral concentrations. (D) Heatmap of the analyses of 23 SARS-CoV-2 aerosol samples and 23 surface swabs of air outlets collected from isolation wards of COVID-19 patients and 12 negative samples. (E) Statistical results of aerosol and aerosol-related samples indicates that the positive detection rate of the SIAMs was approximately three times that of the commercial kit. ND: Not detectable.

a real setting, we next analyzed 23 aerosol samples. By using our system, we achieved a positive rate of 85.7% (18/21), which was notably higher than the 8.7% (2/23) of the commercial kit based on RT-PCR (Fig. 6D and E). We further analyzed surface swab specimens collected from air outlets in the isolating ward of these COVID-19 patients, where the aerosol particles are most likely to be deposited. Using our testing system, we identified 11 (11/13, 84.6%) surface swab samples that were significantly higher than those of the commercial kit (6/23, 26%). Overall, these data demonstrate the practical effectiveness and outstanding performance of SIAMs, which provide a superior platform for environmental monitoring.

Based on the outstanding performance of our platform and the urgent need for aerosol monitoring, we envision wide usage of SIAMs in the following application scenarios: (i) Routine monitoring of SARS-CoV-2 aerosols at places where crowds congregate such as theatres, markets, conference rooms, and offices, instead of testing each individual, to maintain the normal running of the economy and society without disturbance under the prospect of the long-term coexistence with SARS-CoV-2; (ii) Monitoring SARS-CoV-2 aerosols at high-risk places such as fever clinics, isolation hospitals, and isolation hotels, to find loopholes in the epidemic prevention and lower the risks of secondary transmission; (iii) Monitoring SARS-CoV-2 aerosols at places where passengers congregate such as airports, railway stations, subway stations, cruise ships, and border ports, to break the cross-border transmission of COVID-19; (iv) Routine monitoring of SARS-CoV-2 aerosols in logistics centers such as customs, express distribution centers, warehouses, and refrigerated transportation chains, for monitoring and controlling the SARS-CoV-2 transmission through transportation and logistics.

4. Conclusion

In the fight against the COVID-19 pandemic, there exists a constant balance between effective control of COVID-19 outbreaks and the economic price of the preventive measures. Instead of testing each individual, the monitoring of aerosols in a public space is analogous to grouping all people for a single test. As a result, the costs can be significantly reduced and the disturbance to normal activities can be minimized. The sensitivity of this indirect testing of a person should be extremely high to eliminate false-negative results. Using SIAMs, we achieved the detection of 20 copies/mL of SARS-CoV-2 RNA within 25 min and demonstrated the outstanding performance of iCASA using a total of 105 COVID-19 samples. By enhancing the sensitivity of amplification testing, shortening the assay time, and enclosing the testing streamline into a fully integrated chip, we have taken a step toward the automatic detection of viral aerosols for fighting against future pandemics of unknown infectious diseases. Nevertheless, facing the commercialization of the SIAMs, additional advances are still required. In the SIAMs, the aerosol sample still needs to transfer from the aerosol sampler to the chip, and the integration of aerosol sampling into our microfluidic chip will further increase the immediacy of aerosol monitoring and reduce the demand for personnel.

CRediT authorship contribution statement

Shanglin Li: Investigation, Conceptualization, Methodology, Data curation, Formal analysis, Validation, Writing – original draft, Formal analysis. **Bao Li:** Investigation, Conceptualization, Methodology, Data curation, Formal analysis, Validation, Writing – original draft, Formal analysis. **Xinyue Li:** Conceptualization, Methodology, Data curation, Formal analysis, Validation. **Ce Liu:** Investigation, Methodology, Data curation, Formal analysis, Validation. **Xiao Qi:** Formal analysis, Validation. **Yin Gu:** Methodology, Investigation. **Baobao Lin:** Methodology, Investigation. **Lingli Sun:** Methodology, Validation. **Lan Chen:** Investigation, Validation. **Bingqian Han:** Investigation, Methodology. **Jiazhen Guo:** Methodology, Validation. **Yanyi Huang:** Resources, Funding acquisition. **Shuangsheng Wu:** Supervision, Validation, Resources. **Lili Ren:** Supervision, Formal analysis, Resources. **Jianbin Wang:** Supervision, Formal analysis, Funding acquisition. **Jingwei Bai:** Supervision, Formal analysis, Investigation, Validation. **Jianxin Ma:** Supervision, Formal analysis, Validation, Resources, Investigation. **Maosheng Yao:** Supervision, Funding acquisition, Investigation, Resources. **Peng Liu:** Project administration, Conceptualization, Funding acquisition, Formal analysis, Investigation, Writing – review & editing.

Declaration of competing interest

The authors declare that they have no known competing financial interests or personal relationships that could have appeared to influence the work reported in this paper.

Data availability

No data was used for the research described in the article.

Acknowledgments

We thank Dr. Xiaoliang Sunney Xie and his colleagues from the Beijing Changping Laboratory for providing the P2 laboratory, equipment, and financial support. We thank Dr. Ronghua Jin and his colleagues from the Beijing Ditan Hospital, Capital Medical University, for providing clinical samples. This work was funded by Beijing Science and Technology Plans (Z201100009420004 and Z201100007920014) from the Beijing Municipal Science & Technology Commission, China, Tsinghua University Spring Breeze Fund (Grant No. 20201080538), National Natural Science Foundation of China (Grant No. 32001021), State Key Laboratory of Space Medicine Fundamentals and Application (Grant NO. SMFA19C04) from China Astronaut Research and Training Center, and the Opening Foundation of the State Key Laboratory of Space Medicine Fundamentals and Application (Grant NO. SMFA20K01) from Chinese Astronaut Research and Training Center.

Appendix A. Supplementary data

Supplementary data to this article can be found online at https://doi.org/10.1016/j.bios.2022.114816.

References

Alsved, M., Matamis, A., Bohlin, R., Richter, M., Bengtsson, P.E., Fraenkel, C.J., Medstrand, P., Löndahl, J., 2020. Aerosol Sci. Technol. 54 (11), 1245–1248.
Bastos, M.L., Perlman-Arrow, S., Menzies, D., Campbell, J.R., 2021. Ann. Intern. Med. 174 (4), 501–510.
Chaibun, T., Puenpa, J., Ngamdee, T., Boonapatcharoen, N., Athamanolap, P., O'Mullane, A.P., Vongpunsawad, S., Poovorawan, Y., Lee, S.Y., Lertanantawong, B., 2021. Nat. Commun. 12 (1), 802.
Cherkaoui, D., Huang, D., Miller, B.S., Turbé, V., McKendry, R.A., 2021. Biosens. Bioelectron. 189, 113328.
Chu, H., Chan, J.F., Wang, Y., Yuen, T.T., Chai, Y., Hou, Y., Shuai, H., Yang, D., Hu, B., Huang, X., Zhang, X., Cai, J.P., Zhou, J., Yuan, S., Kok, K.H., To, K.K., Chan, I.H., Zhang, A.J., Sit, K.Y., Au, W.K., Yuen, K.Y., 2020. Clin. Infect. Dis. 71 (6), 1400–1409.
Esbin, M.N., Whitney, O.N., Chong, S., Maurer, A., Darzacq, X., Tjian, R., 2020. RNA 26 (7), 771–783.
Gan, W., Gu, Y., Han, J., Li, C.X., Sun, J., Liu, P., 2017. Anal. Chem. 89 (6), 3568–3575.
Geng, Z., Gu, Y., Li, S., Lin, B., Liu, P., 2019. Micromachines 10 (12), 873.
Geng, Z., Li, S., Zhu, L., Cheng, Z., Jin, M., Liu, B., Guo, Y., Liu, P., 2020. Anal. Chem. 92 (10), 7240–7248.
Gu, Y., Zhuang, B., Han, J., Li, Y., Song, X., Zhou, X., Wang, L., Liu, P., 2019. Anal. Chem. 91 (11), 7435–7443.
He, Y., Xie, T., Tong, Y., 2021. Biosens. Bioelectron. 187, 113330.
Holshue, M.L., DeBolt, C., Lindquist, S., Lofy, K.H., Wiesman, J., Bruce, H., Spitters, C., Ericson, K., Wilkerson, S., Tural, A., Diaz, G., Cohn, A., Fox, L., Patel, A., Gerber, S.I., Kim, L., Tong, S., Lu, X., Lindstrom, S., Pallansch, M.A., Weldon, W.C., Biggs, H.M., Uyeki, T.M., Pillai, S.K., 2020. N. Engl. J. Med. 382 (10), 929–936.
Höss, M., Pääbo, S., 1993. Nucleic Acids Res. 21 (16), 3913–3914.
Karim, S.S.A., Karim, Q.A., 2021. Lancet 398 (10317), 2126–2128.
Li, X., Chen, H., Qi, X., Peng, Y., Zhou, L., Ma, J., Yao, M., 2021a. Aerosol Air Qual. Res. 21 (12), 210130.

Li, Z., Bai, Y., You, M., Hu, J., Yao, C., Cao, L., Xu, F., 2021b. Biosens. Bioelectron. 177, 112952.
Liu, Y., Ning, Z., Chen, Y., Guo, M., Liu, Y., Gali, N.K., Sun, L., Duan, Y., Cai, J., Westerdahl, D., Liu, X., Xu, K., Ho, K.F., Kan, H., Fu, Q., Lan, K., 2020. Nature 582 (7813), 557–560.
Milton, D.K., 2020. J. Pediatric Infect. Dis. Soc. 9 (4), 413–415.
Morawska, L., Johnson, G.R., Ristovski, Z.D., Hargreaves, M., Mengersen, K., Corbett, S., Chao, C.Y.H., Li, Y., Katoshevski, D., 2009. J. Aerosol Sci. 40 (3), 256–269.
Morawska, L., Milton, D.K., 2020. Clin. Infect. Dis. 71 (9), 2311–2313.
Planas, D., Veyer, D., Baidaliuk, A., Staropoli, I., Guivel-Benhassine, F., Rajah, M.M., Planchais, C., Porrot, F., Robillard, N., Puech, J., Prot, M., Gallais, F., Gantner, P., Velay, A., Le Guen, J., Kassis-Chikhani, N., Edriss, D., Belec, L., Seve, A., Courtellemont, L., Pere, H., Hocqueloux, L., Fafi-Kremer, S., Prazuck, T., Mouquet, H., Bruel, T., Simon-Loriere, E., Rey, F.A., Schwartz, O., 2021. Nature 596 (7871), 276–280.
Pokhrel, P., Hu, C., Mao, H., 2020. ACS Sens. 5 (8), 2283–2296.
Prather, K.A., Wang, C.C., Schooley, R.T., 2020. Science 368 (6498), 1422–1424.
Sawano, M., Takeshita, K., Ohno, H., Oka, H., 2021. J. Breath Res. 15 (3), 037103.
Shaw, K.J., Thain, L., Docker, P.T., Dyer, C.E., Greenman, J., Greenway, G.M., Haswell, S.J., 2009. Anal. Chim. Acta 652 (1–2), 231–233.
Stadnytskyi, V., Bax, C.E., Bax, A., Anfinrud, P., 2020. Proc. Natl. Acad. Sci. U. S. A. 117 (22), 11875–11877.
van Doremalen, N., Bushmaker, T., Morris, D.H., Holbrook, M.G., Gamble, A., Williamson, B.N., Tamin, A., Harcourt, J.L., Thornburg, N.J., Gerber, S.I., Lloyd-Smith, J.O., de Wit, E., Munster, V.J., 2020. N. Engl. J. Med. 382 (16), 1564–1567.